

Emulating complex dynamical simulators with random Fourier features

Hossein Mohammadi^{*1}, Peter Challenor¹, and Marc Goodfellow^{1, 2}

¹College of Engineering, Mathematics and Physical Sciences, University of Exeter, Exeter, UK

²Living Systems Institute, University of Exeter, Exeter, UK

Abstract

A Gaussian process (GP)-based methodology is proposed to emulate complex dynamical computer models (or simulators). The method relies on emulating the short-time numerical flow map of the system, where the flow map is a function that returns the solution of a dynamical system at a certain time point, given initial conditions. Here, the flow map is emulated via a GP whose kernel is approximated with random Fourier features. This yields a random predictor whose realisations are approximations to the flow map. In order to predict a given time series (i.e., the model output), a single realisation of the approximate flow map is taken and used to iterate from the initial condition ahead in time. Repeating this procedure with multiple realisations from the distribution of approximate flow maps creates a distribution over the time series whose mean and variance serve as the model output prediction and the associated uncertainty, respectively. The proposed method is applied to emulate several dynamic nonlinear simulators including the well-known Lorenz and van der Pol models. The results suggest that our approach has a high predictive performance and the associated uncertainty can capture the dynamics of the system accurately. Additionally, our approach has potential for “embarrassingly” parallel implementations where one can conduct the iterative predictions performed by a realisation on a single computing node.

Keywords: Dynamical simulator; Emulation; Gaussian process; Random Fourier features

1 Introduction

The problem of predicting the output of complex computer codes (or simulators) occurs frequently in many real-world applications [25, 53]. Such

^{*}Corresponding author: h.mohammadi@exeter.ac.uk

simulators are based on complicated mathematical equations and can be computationally intensive. Hence the number of simulation runs is limited by our budget for computation. One way to overcome this problem is to create a surrogate of the computer code which is cheap-to-evaluate. Surrogates are statistical representation of the true model and are constructed based on a limited number of simulation runs. A survey of the most widely used surrogate models is presented in [1, 26]. Among broad types of surrogate models, Gaussian process (GP) emulators [42] have become the gold standard in the field of the design and analysis of computer experiments [12, 45, 46]. This is due to their statistical properties such as the flexibility and computational tractability, see Section 2 for further detail, though other methods from machine learning such as neural networks are also used [53].

In this work, we focus on the emulation of deterministic *dynamical simulators* which are based on a set of ordinary differential equations (ODE). Dynamical simulators are an important class of computer codes whose output is a time series. They simulate the evolution of a physical process over time and are widely used in various fields including biology [43] and climate science [44]. The Hindmarsh-Rose (HR) model [23], which simulates the dynamics of a single neuron, is a specific example that is discussed in more detail in Section 5.3.

Emulating dynamical computer codes is an active field of research and has been tackled via different statistical and machine learning approaches, see e.g. [7, 10, 11, 37, 41]. One may consider this problem as a special case of multi-output GPs [2, 14, 19] with a temporal dependency between the observations. However, the size of the output dimension in dynamical models is usually too high to be treated through multi-output GPs. To address this issue, one can first apply techniques such as principal component analysis [22, 25] or wavelet decomposition [4, 16] to reduce the output dimensionality. The pitfall is that we lose some information by not keeping all the components. Another approach is proposed in [28] which accounts for time using an extra input parameter. This method increases the computational complexity and is reported to be inefficient [13, 35]. The idea of forecasting the time series through iterative one-step ahead predictions is developed in [5, 13]. This method relies on emulating the transition function from one time point to the next, under the assumption that the model output at time t depends only on the observation at time $t - 1$, i.e. the Markov property. The work is continued in [37] considering the input uncertainty at each step of the iterative prediction process.

This paper presents a novel data-driven approach for emulating complex dynamical simulators relying on emulating the numerical flow map over a short period of time. The flow map is a function that maps an initial condition to the solution of the system at a certain time point. We emulate the short-time numerical flow map of the system by a GP whose kernel is approximated with random Fourier features (RFF) [40]. This yields a

random predictor to the flow map. In order to predict the time series, a realisation from the approximate flow map is drawn and used in an iterative manner to perform one-step ahead predictions. By repeating this procedure with multiple draws, we acquire a distribution over the time series whose mean and variance serve as the model output prediction and the associated uncertainty, respectively. The results show that our method has a high prediction accuracy and the associated uncertainty can capture the true trajectory with a good precision.

The rest of the paper is organised as follows. First, we give a brief overview of dynamical systems. Then, in Section 2 we introduce GP emulators. Section 3 reviews RFF and its application to kernel approximation and GPs. Section 4 describes our proposed method for emulating dynamical models. Numerical results are provided in Section 5 where we apply our method to emulate several dynamical systems. Finally, Section 6 presents our conclusions.

Dynamical system A dynamical system represents the evolution of a phenomenon over time according to a fixed mathematical rule. Here we focus on continuous time systems represented by a set of ordinary differential equations, hence solutions of these equations are given by the vector of *state variables*, $\mathbf{x}(t) = (x_1(t), \dots, x_d(t))^\top$ which determines the state of the system at time $t \in \mathbb{R}$. The space that consists of all possible values of the state variables is called the *state (phase) space* denoted by $\mathcal{X} \subset \mathbb{R}^d$. The ordinary differential equations define a *vector field*, v , in \mathbb{R}^d , that is tangent to the solution [50], i.e.

$$v : \mathcal{X} \mapsto \mathcal{X}, \quad \frac{d}{dt}\mathbf{x}(t) = v(\mathbf{x}(t)). \quad (1)$$

We assume that the system is autonomous meaning that the associated vector field does not depend on time explicitly.

Let \mathbf{x}_0 be an initial condition, which represents the state of the system at an initial time t_0 , and Δt a time step. The *flow map* (F) is a function that maps \mathbf{x}_0 to the state at the next time step $t_1 = t_0 + \Delta t$ [15]:

$$F : \mathcal{X} \times \mathbb{R} \mapsto \mathcal{X}, \quad F(\mathbf{x}_0, \Delta t) = \mathbf{x}(t_1). \quad (2)$$

The flow map can be interpreted as mapping the initial condition to the end point of a short trajectory traced out in the state space from \mathbf{x}_0 to $\mathbf{x}(t_1)$. In this work, we assume that the time step Δt is fixed, and hence the flow map is a function of \mathbf{x}_0 only.

2 Gaussian process emulators

Our aim is to build statistical representations of the flow map based on GPs to enable efficient construction of trajectories with quantified uncertainty.

The potential benefits of this approach are shown in [37]. Before explaining the advances in the current manuscript, we introduce GP emulators.

Let $f(\mathbf{x})$, $\mathbf{x} \in \mathcal{X}$, be the function we wish to emulate. We do this using the stochastic Gaussian process $Y(\mathbf{x})$ given by

$$Y(\mathbf{x}) = \mu(\mathbf{x}) + Z(\mathbf{x}), \quad (3)$$

in which $\mu : \mathcal{X} \mapsto \mathbb{R}$ is the *trend function* that can take any functional form. In this work, the trend function is linear $\mu(\mathbf{x}) = \mathbf{q}(\mathbf{x})^\top \boldsymbol{\beta}$ with $\mathbf{q}(\mathbf{x}) = [q_1(\mathbf{x}), \dots, q_r(\mathbf{x})]^\top$ and $\boldsymbol{\beta} = [\beta_1, \dots, \beta_r]^\top$ being the vector of basis (regression) functions and the corresponding coefficients, respectively. The second component in Equation (3), $Z(\mathbf{x})$, is a centred (or zero mean) GP with the covariance function

$$\text{Cov}(Z(\mathbf{x}), Z(\mathbf{x}')) = \sigma^2 k(\mathbf{x}, \mathbf{x}'), \quad \forall \mathbf{x}, \mathbf{x}' \in \mathcal{X}. \quad (4)$$

The scalar σ^2 is the *process (signal) variance* and controls the scale of the amplitude of $Z(\mathbf{x})$. The function $k : \mathcal{X} \times \mathcal{X} \mapsto \mathbb{R}$ is the kernel or correlation function and regulates the level of smoothness of $Z(\mathbf{x})$. A kernel is called *stationary (shift invariant)* if it depends only on the difference between its inputs: $k(\mathbf{x}, \mathbf{x}') = k(\mathbf{x} - \mathbf{x}')$. One of the most common stationary correlation functions is the squared exponential (SE) kernel defined as [42]

$$k_{SE}(\mathbf{x}, \mathbf{x}') = \exp\left(-0.5 (\mathbf{x} - \mathbf{x}')^\top \boldsymbol{\Delta}^{-2} (\mathbf{x} - \mathbf{x}')\right), \quad (5)$$

where the diagonal matrix $\boldsymbol{\Delta} \in \mathbb{R}^{d \times d}$ consists of the *correlation length-scales* denoted by $\delta_1, \dots, \delta_d$.

Let $\mathcal{D} = \{\mathbf{X}, \mathbf{y}\}$ denote the training data set in which $\mathbf{X} = [\mathbf{x}^1, \dots, \mathbf{x}^n]^\top$ is called the *design matrix* and includes n points in the input space. The vector $\mathbf{y} = [f(\mathbf{x}^1), \dots, f(\mathbf{x}^n)]^\top$ comprises the outputs at those locations. For our purpose, $\mathbf{x}^1, \dots, \mathbf{x}^n$ represent samples taken from the state space and are used to build an emulator for the flow map, as described in Section 4. Typically, GPs are presented from a *function space* perspective where the predictive distribution relies on the posterior $Y(\mathbf{x}) \mid \mathcal{D}$. However, GPs can be interpreted from a *weight space* perspective in which $Z(\mathbf{x})$ is expressed by [42]

$$Z(\mathbf{x}) = \boldsymbol{\phi}(\mathbf{x})^\top \mathbf{w}, \quad \boldsymbol{\phi}(\mathbf{x}) = [\phi_1(\mathbf{x}), \phi_2(\mathbf{x}), \dots]^\top, \quad (6)$$

that is a weighted sum of (possibly infinite) basis functions. The vector \mathbf{w} consists of the weights and $\boldsymbol{\phi}(\mathbf{x}) : \mathcal{X} \mapsto \mathcal{H}$ is called the *feature map* and transforms the input space into a reproducing kernel Hilbert space (RKHS) \mathcal{H} [38]. It is shown that the inner product between $\boldsymbol{\phi}(\mathbf{x})$ and $\boldsymbol{\phi}(\mathbf{x}')$ on \mathcal{H} can be computed using the kernel k as $\langle \boldsymbol{\phi}(\mathbf{x}), \boldsymbol{\phi}(\mathbf{x}') \rangle_{\mathcal{H}} = k(\mathbf{x}, \mathbf{x}')$ [47, 24]. A brief overview of RKHSs is provided in Appendix A. Given that all parameters

in (3) are known, the predictive mean in the weight space view takes the following form [51]

$$\tilde{f}(\mathbf{x}) = \mu(\mathbf{x}) + \phi(\mathbf{x})^\top \Phi \left(\Phi^\top \Phi \right)^{-1} (\mathbf{y} - \boldsymbol{\mu}), \quad (7)$$

where $\boldsymbol{\mu} = \mu(\mathbf{X})$ and $\Phi = [\phi(\mathbf{x}^1), \dots, \phi(\mathbf{x}^n)]$ is the aggregation of columns of $\phi(\mathbf{x})$ for all points in the training set [42]. Equation (7) is obtained by assuming a Gaussian distribution over \mathbf{w} and computing its posterior [38, 42, 51]. The weight space representation of GPs is particularly advantageous for purposes of drawing samples from their predictive mean [55]. This is the driving idea behind the present paper and is described in more detail next.

3 RFF approximation and GPs

This section provides the material necessary for approximating a kernel with RFF. The predictive mean of a GP whose kernel is approximated this way is random allowing us to draw realisations from its distribution. This idea is used in Section 4 to emulate the numerical flow map of dynamical systems and predict their output. The other applications of kernel approximation with RFF can be found in Bayesian optimisation [48], deep learning [36], and big data modelling [33]. We start the discussion by introducing RFF rigorously.

3.1 Kernel approximation with RFF

RFF offers an effective solution to approximate stationary kernels relying on Bochner’s theorem [6]. According to this theorem, the Fourier transform of the stationary kernel k is

$$k(\mathbf{x}, \mathbf{x}') = \int e^{-i\boldsymbol{\omega}^\top (\mathbf{x} - \mathbf{x}')} d\mathbb{P}(\boldsymbol{\omega}), \quad (8)$$

where $\mathbb{P}(\boldsymbol{\omega})$ (the Fourier dual of k) is equal to the *spectral density* of the kernel. $\mathbb{P}(\boldsymbol{\omega})$ has all the properties of a cumulative distribution function except that $\mathbb{P}(\infty) - \mathbb{P}(-\infty) = k(\mathbf{0})$ needs not to be equal to one [32]. However, in classic correlation functions such as the SE kernel, $\mathbb{P}(\boldsymbol{\omega})$ is a proper cumulative distribution function because $k(\mathbf{0}) = 1$. In this situation, $p(\boldsymbol{\omega}) = \frac{d\mathbb{P}(\boldsymbol{\omega})}{d\boldsymbol{\omega}}$ is the density function of $\boldsymbol{\omega}$ and Equation (8) can be rewritten as [21]

$$\begin{aligned} k(\mathbf{x}, \mathbf{x}') &= \int e^{-i\boldsymbol{\omega}^\top (\mathbf{x} - \mathbf{x}')} p(\boldsymbol{\omega}) d\boldsymbol{\omega} = \mathbb{E}_{p(\boldsymbol{\omega})} \left[e^{-i\boldsymbol{\omega}^\top (\mathbf{x} - \mathbf{x}')} \right] \\ &= \mathbb{E}_{p(\boldsymbol{\omega})} \left[\text{Re} \left(e^{-i\boldsymbol{\omega}^\top \mathbf{x}} (e^{-i\boldsymbol{\omega}^\top \mathbf{x}'})^* \right) \right] \\ &= \mathbb{E}_{p(\boldsymbol{\omega})} \left[\varphi(\mathbf{x})^\top \varphi(\mathbf{x}') \right]. \end{aligned} \quad (9)$$

Here, the superscript $*$ denotes the complex conjugate and $\varphi(\cdot)$ is a random feature map. Note that the imaginary component is not required since we only work with real-valued kernels. A possible choice for $\varphi(\cdot)$ is

$$\varphi(\mathbf{x}) = \sqrt{2} \cos \left(\boldsymbol{\omega}^\top \mathbf{x} + b \right), \quad (10)$$

in which $b \sim \mathcal{U}[0, 2\pi]$ is a uniform random variable [40, 21]. The distribution of $\boldsymbol{\omega}$ depends on the type of correlation function. For example, the spectral density $p(\boldsymbol{\omega})$ of the Matérn kernel is a t -distribution and for the SE kernel is Gaussian specified by [40, 54]

$$\boldsymbol{\omega}_{SE} \sim \mathcal{N}(\mathbf{0}, \boldsymbol{\Delta}^{-2}). \quad (11)$$

The explicit random feature map $\varphi(\mathbf{x})$ defined by Equation (10) allows us to estimate the (actual) feature map $\boldsymbol{\phi}(\mathbf{x})$, which is possibly infinite dimensional. This can be performed using a Monte Carlo approach where we generate M independently and identically distributed (i.i.d.) samples from $p(\boldsymbol{\omega})$ and $p(b) = \mathcal{U}[0, 2\pi]$ denoted by $\boldsymbol{\omega}^{(1)}, \dots, \boldsymbol{\omega}^{(M)}$ and $b^{(1)}, \dots, b^{(M)}$, respectively. Then, the approximated feature map $\hat{\boldsymbol{\phi}}(\mathbf{x})$ is achieved by

$$\hat{\boldsymbol{\phi}}(\mathbf{x}) = \sqrt{\frac{2}{M}} \left[\cos \left(\boldsymbol{\omega}^{(1)\top} \mathbf{x} + b^{(1)} \right), \dots, \cos \left(\boldsymbol{\omega}^{(M)\top} \mathbf{x} + b^{(M)} \right) \right]^\top, \quad (12)$$

which transforms an input vector \mathbf{x} into the M -dimensional feature space. Finally, the stationary kernel k is approximated as

$$k(\mathbf{x}, \mathbf{x}') = \mathbb{E}_{p(\varphi)} \left[\varphi(\mathbf{x})^\top \varphi(\mathbf{x}') \right] \approx \hat{\boldsymbol{\phi}}(\mathbf{x})^\top \hat{\boldsymbol{\phi}}(\mathbf{x}'). \quad (13)$$

It is worth mentioning that the quality of the above approximation is

$$\sup_{\mathbf{x}, \mathbf{x}' \in \mathcal{X}} \left| k(\mathbf{x}, \mathbf{x}') - \hat{\boldsymbol{\phi}}(\mathbf{x})^\top \hat{\boldsymbol{\phi}}(\mathbf{x}') \right| \leq \varepsilon, \quad (14)$$

where $\varepsilon := \mathcal{O}(M^{-1/2})$ [40].

3.2 GP prediction with RFF

The predictive mean of a GP whose kernel is approximated with RFF takes the following form

$$\hat{f}(\mathbf{x}) = \mu(\mathbf{x}) + \hat{\boldsymbol{\phi}}(\mathbf{x})^\top \hat{\mathbf{\Phi}} \left(\hat{\mathbf{\Phi}}^\top \hat{\mathbf{\Phi}} \right)^{-1} (\mathbf{y} - \boldsymbol{\mu}), \quad (15)$$

wherein $\hat{\mathbf{\Phi}} = \left[\hat{\boldsymbol{\phi}}(\mathbf{x}^1), \dots, \hat{\boldsymbol{\phi}}(\mathbf{x}^n) \right]$ is an $M \times n$ -dimensional matrix and estimates $\mathbf{\Phi}$. Since the construction of $\hat{\boldsymbol{\phi}}(\mathbf{x})$ (see Equation (12)) relies on i.i.d. samples taken from the kernel spectral density $p(\boldsymbol{\omega})$ and $p(b)$, the predictive

mean in (15) is stochastic and its s -th realisation is denoted by $\hat{f}^{(s)}(\mathbf{x})$. By repeating the Monte Carlo sampling scheme, we can generate multiple such realisations. This idea is used to emulate dynamical simulators where multiple draws from the approximate flow map are employed to perform one-step ahead predictions. With this, one can quantify uncertainty of the time series prediction in the absence of a closed-form expression. See the next section for more details on this. The procedure to approximate the predictive mean with RFF is outlined in Algorithm 1.

Algorithm 1 GP with RFF approximation

Input: training set $\{\mathbf{X}, \mathbf{y}\}$, trend function μ , kernel spectral density $p(\omega)$, dimension of random feature space M

- 1: Draw M i.i.d. samples from $p(\omega)$ and $p(b) = \mathcal{U}[0, 2\pi]$
 - 2: Compute $\hat{\phi}(\mathbf{x})$ using Equation (12)
 - 3: Construct $\hat{\Phi} = [\hat{\phi}(\mathbf{x}^1), \dots, \hat{\phi}(\mathbf{x}^n)]$
 - 4: Compute $\hat{f}(\mathbf{x})$ using Equation (15)
-

4 Emulating dynamical simulators

Now let us introduce our methodology for emulating deterministic non-linear dynamical simulators that are based on ODE. Let $\mathbf{x}(t_1) = (x_1(t_1), \dots, x_d(t_1))^\top$ denote the solution of the system at $t_1 = t_0 + \Delta t$ for a given fixed “small” time step Δt and initial condition \mathbf{x}_0 . We assume that $\mathbf{x}(t_1)$ is produced by the flow map F defined as

$$F(\mathbf{x}_0) = (f_1(\mathbf{x}_0), \dots, f_d(\mathbf{x}_0))^\top = (x_1(t_1), \dots, x_d(t_1))^\top, \quad (16)$$

such that each map $f_i : \mathcal{X} \mapsto \mathbb{R}$ yields the i -th component of $\mathbf{x}(t_1)$, i.e. $x_i(t_1)$. A prediction associated with the dynamics of $x_i(t)$ is achieved by:

- Emulating f_i by a GP with RFF approximation, \hat{f}_i
- Drawing a realisation from \hat{f}_i using Algorithm 1, $\hat{f}^{(s)}$
- Using $\hat{f}^{(s)}$ iteratively to perform one-step ahead predictions

Following the above procedure renders only one prediction to the time series. However, we wish to have an estimation of uncertainty associated with the prediction accuracy. This can be achieved by repeating the above steps with different draws from the emulated flow map to reach a distribution over the time series. The mean and variance of that distribution then serve as the model output prediction and the associated uncertainty, respectively. Our proposed emulation method is summarised in Algorithm 2 where $\hat{f}_i^{(s)}(\mathbf{x})$

stands for the s -th approximation to the predictive mean of the GP obtained by RFF and used to emulate $f_i(\mathbf{x})$.

The first step in Algorithm 2 is to choose n sample points denoted by $\mathbf{X} = \{\mathbf{x}_0^1, \dots, \mathbf{x}_0^n\}$ from the space of initial conditions \mathcal{X} . These points have a substantial effect on the accuracy of emulators and are selected in a carefully designed experiment. In this work, \mathbf{X} is obtained through a “space-filling” sampling strategy where the samples fill the space uniformly. A space-filling design can be achieved via techniques such as Latin hypercube sampling (LHS) [27, 18]. Interested readers are referred to [45, 46] for more information on space-filling designs.

5 Numerical results

The prediction performance of our proposed method is tested on several dynamical systems implemented as computer codes. They are the Lorenz [34], van der Pol [50], and Hindmarsh-Rose models [23] and are further elaborated in the following subsections. The training data set consists of $n = 15 \times d$ space-filling points selected from the space of initial conditions. We use the `optimumLHS` function implemented in the R package `lhs` [9] to sample the initial conditions. The `optimumLHS` function maximises the mean distance between all candidate points.

The GP correlation function is the squared exponential kernel as is recommended in [13, 37]. The trend function is a first order regression model: $\mu(\mathbf{x}) = \beta_1 + \beta_2 \mathbf{x}$. The coefficients β_1 and β_2 together with the covariance function parameters such as the length-scales $(\delta_1, \dots, \delta_d)$ and process variance (σ^2) are estimated using maximum likelihood, see Appendix B. The dimensionality of the random feature space is $M = 250$ as is considered in [21]. The number of realisations drawn from the approximate flow map is $S = 100$. The simulation time step is fixed and equal to $\Delta t = 0.01$. The

Algorithm 2 Emulating dynamic non-linear simulators

- 1: Select n space-filling initial conditions: $\mathbf{X} = \{\mathbf{x}_0^1, \dots, \mathbf{x}_0^n\}$
 - 2: Run the simulator for each $\mathbf{x}_0^1, \dots, \mathbf{x}_0^n$ over Δt to obtain
 $\mathbf{y} = \{\mathbf{x}^1(t_1), \dots, \mathbf{x}^n(t_1)\}$
 - 3: **for** $i = 1$ to d **do**
 - 4: Create $\mathcal{D}_i = \{\mathbf{X}, \mathbf{y}_i\}$ where $\mathbf{y}_i = (x_i^1(t_1), \dots, x_i^n(t_1))^\top$
 - 5: **for** $s = 1$ to S **do**
 - 6: Generate $\hat{f}_i^{(s)}(\mathbf{x})$ using Algorithm 1
 - 7: Use $\hat{f}_i^{(s)}(\mathbf{x})$ iteratively to perform one-step ahead predictions
 - 8: **end for**
 - 9: Calculate the mean and variance of the S time series
 - 10: **end for**
-

ODE is solved by the default solver of the R package `deSolve` [49].

The accuracy of the time series prediction is measured via the *mean absolute error (MAE)* and *root mean square error (RMSE)* criteria defined as

$$MAE = \frac{\sum_{t=1}^{t=T} |x(t) - \hat{x}(t)|}{n_{step}}, \quad (17)$$

$$RMSE = \sqrt{\frac{\sum_{t=1}^{t=T} (x(t) - \hat{x}(t))^2}{n_{step}}}. \quad (18)$$

Here, T is the final time of the simulation and $n_{step} = T/\Delta t$ denotes the total number of one-step ahead predictions. We compare our results with the method presented in [37] as it is also based on emulating the numerical flow map and one-step ahead predictions. We refer to our proposed approach as “Method 1” and that of [37] as “Method 2” in the rest of the paper.

5.1 Lorenz system

The Lorenz system was initially derived by Edward Lorenz in 1963 [34]. Although it was originally developed as a model of convection in the earth’s atmosphere, the Lorenz system has applications to other fields, see e.g. [39]. This model can produce a famous chaotic attractor whereby trajectories on the attractor are very sensitive to initial conditions. In other words, the difference in evolution of the system starting from two slightly different points will become large. The Lorenz equations are

$$\begin{cases} \frac{dx_1}{dt} = a_1 x_1 + x_2 x_3 \\ \frac{dx_2}{dt} = a_2 (x_2 - x_3) \\ \frac{dx_3}{dt} = -x_1 x_2 + a_3 x_2 - x_3, \end{cases} \quad (19)$$

with the classic parameter values of $a_1 = -8/3$, $a_2 = -10$ and $a_3 = 28$. which are used in our experiments. These values result in the well-know “butterfly attractor” [52].

The predictive performance of Methods 1 and 2 in emulating the Lorenz model is displayed in Figures 1 and 2, respectively. The initial condition in both cases is $\mathbf{x}_0 = (1, 1, 1)^\top$, the red point in the three-dimensional graph. Throughout this paper, the simulation is shown in red, emulation in black and the credible interval (i.e. the prediction \pm standard deviation (SD) of prediction) is represented by the shaded area. The two methods exhibit similar performances and their prediction accuracy is high up to around $t \approx 14$. After that time, the emulator deviates from the true model and tends to the average of the process. At the same time, the prediction uncertainties blow up, which allows the credible interval to encompass most values of the system. However, Method 1 appears to capture the uncertainty better in

that it encompasses all of the trajectory and more tightly follows the fluctuation in dynamics. We note that the Lorenz attractor cannot be predicted perfectly due to its chaotic behaviour. The vertical dashed blue lines indicate the “predictability horizon” defined as the time at which a change point occurs in the SD of prediction [37]. The predictability horizon is acquired by applying the `cpt.mean` function implemented in the R package `changepoint` [29, 30] to the SD of predictions. This is illustrated in Figure 3 which visualises the SD of predictions associated with the state variables x_1 (black) and x_2 (red) obtained by Method 1 in the Lorenz system. The vertical dashed lines are the corresponding change points.

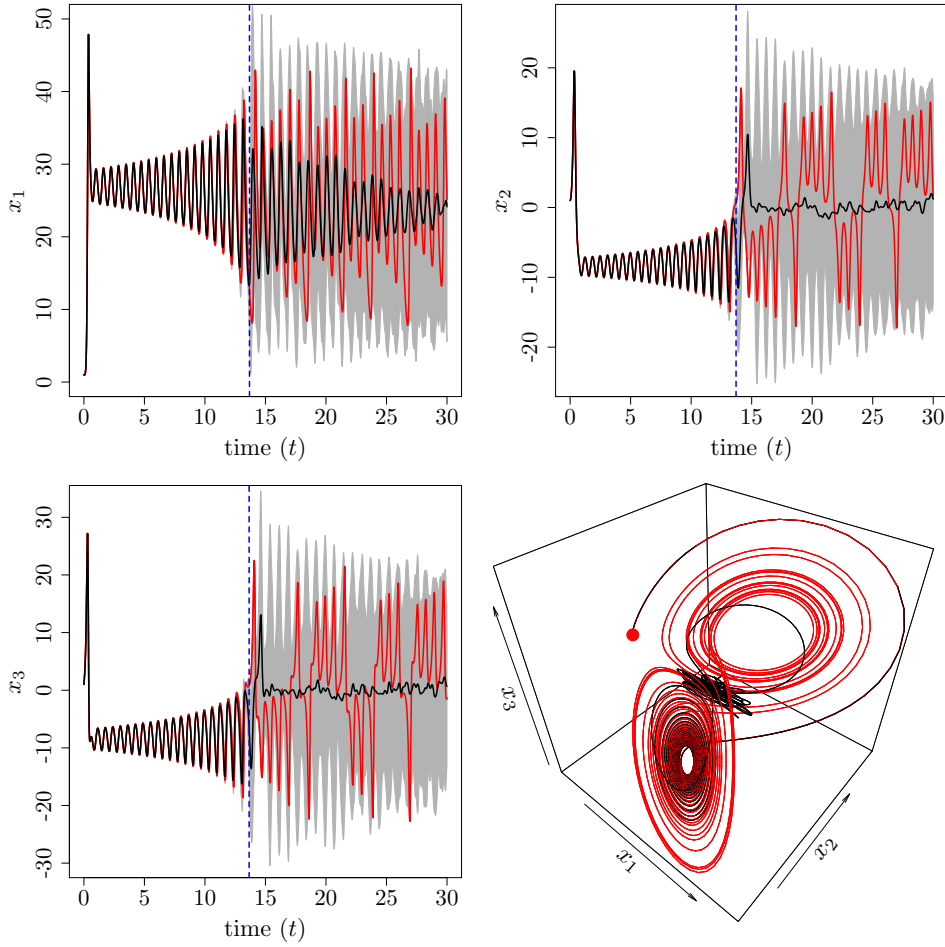


Figure 1: The prediction (black) and associated uncertainty (shaded) in emulating the Lorenz model (red) using Method 1. The initial condition is $\mathbf{x}_0 = (1, 1, 1)^\top$ denoted by a red point in the three-dimensional picture. The vertical dashed blue lines represent the predictability horizon which are the change point in the diagram of prediction uncertainties. The parameter values are $a_1 = -8/3$, $a_2 = -10$ and $a_3 = 28$.

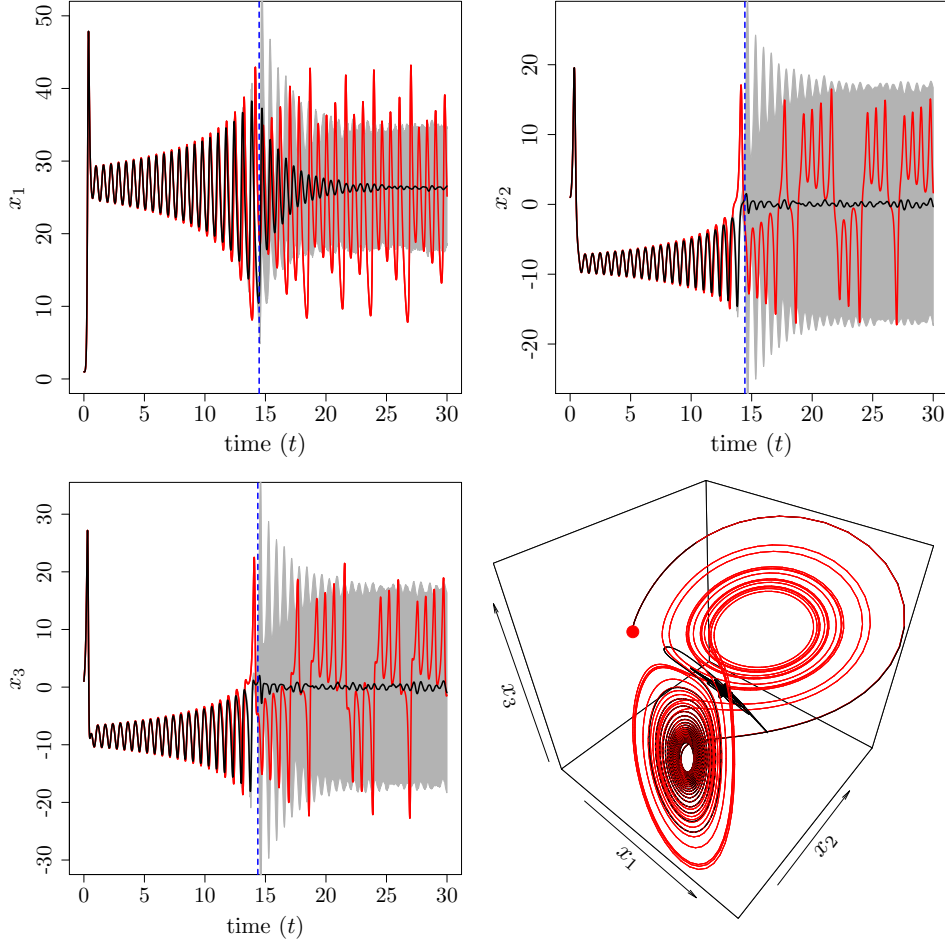


Figure 2: The Lorenz model (red) and its emulation (black) obtained by Method 2. The vertical dashed blue lines show the predictability horizon. The initial condition and the parameter values are the same as Figure 1.

In order to have a more rigorous comparison between the two methods, we compare them based on the RMSE and MAE criteria. To do this, we select randomly 100 initial conditions from $[-10, 10]^3$ and for each initial condition we emulate the model with the two methods. Figure 4 illustrates the results obtained by Methods 1 (green) and 2 (orange). As can be seen, Method 1 has a higher prediction accuracy in emulating the first state variable (x_1) than Method 2. For the second and the third state variables, both methods have similar predictive performances.

5.2 Van der Pol oscillator

The van der Pol equation was first proposed by the Dutch engineer Balthasar van der Pol in 1920 while working on the behaviour of vacuum tube circuits.

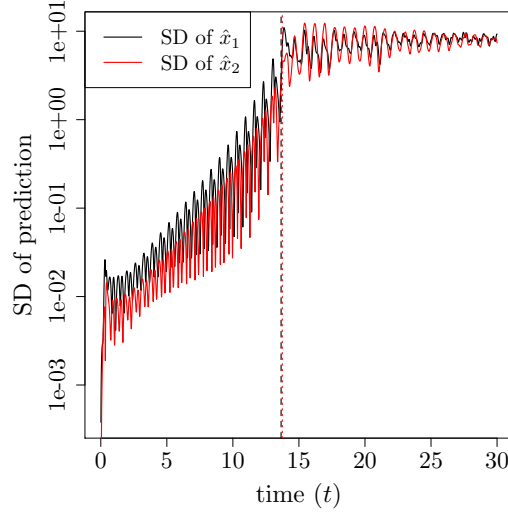


Figure 3: Standard deviation (SD) of prediction associated with the variables x_1 (black) and x_2 (red) obtained by Method 1 in the Lorenz model. The vertical dashed lines show the change point of each diagram. The y-axis is on logarithmic scale.

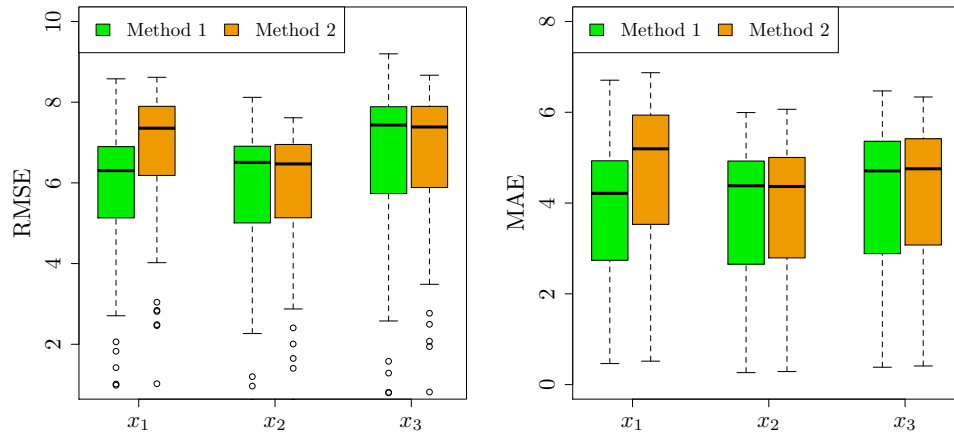


Figure 4: The box plot of the RMSE and MAE criteria in emulating the Lorenz system. The results are achieved using 100 initial conditions selected randomly from $[-10, 10]^3$. The accuracy of Method 1 (green) is higher than Method 2 (orange) in emulating x_1 . However, they perform comparably when predicting x_2 and x_3 .

Since then, this model has been extensively used to study oscillatory phenomena such as the heartbeat [17], biological [56] and circadian rhythms [8]. The evolution of the van der Pol model are [50]

$$\begin{cases} \frac{dx_1}{dt} = x_2 \\ \frac{dx_2}{dt} = a(1 - x_1^2)x_2 - x_1, \end{cases} \quad (20)$$

where the parameter $a > 0$ controls the frequency of oscillations. The van der Pol oscillator exhibits a periodic motion, i.e. a limit cycle.

The emulation of the van der Pol oscillator based on Methods 1 and 2 is visualised in Figures 5 and 6, respectively. The truth (red), prediction (black), credible interval (shaded) and predictability horizon (dashed blue) are illustrated in the figures. The initial condition (the red point in the two-dimensional picture) is $\mathbf{x}_0 = (1, 1)^\top$ and $a = 5$ in both cases. We observe that Method 1 outperforms Method 2 in emulating the van der Pol model. In particular, the first state variable is predicted with a high accuracy by Method 1 and the predictability horizon is equal to the total simulation time. There is a frequency miss-match in the predictions gained by Method 2 after the predictability horizon. Moreover, the amplitude of the predictions (especially \hat{x}_2) gradually dampens. However, such issues are less severe in Method 1. This can be confirmed by Figure 7 in which the two methods are compared based on MAE and RMS. As can be seen, both criteria obtained by Method 1 are notably smaller than those of Method 2 suggesting an improved accuracy in our proposed approach.

5.3 Hindmarsh-Rose model

The Hindmarsh-Rose (HR) model [23] is widely used in biology to study the non-linear dynamics of excitable cells such as neurons. Neurons are specialised cells that are responsible for generating electrical signals called *action potentials*. Information is transmitted via an action potential throughout the nervous system. The HR model is capable of mimicking spiking and bursting which may occur in real cells. The mathematical equations of the HR model are

$$\begin{cases} \frac{dx_1}{dt} = x_2 - a_1x^3 + a_2x^2 - x_3 + I \\ \frac{dx_2}{dt} = a_3 - a_4x_1^2 - x_2 \\ \frac{dx_3}{dt} = \varepsilon (a_5(x_1 - x_{rest}) - x_3). \end{cases} \quad (21)$$

The state variable x_1 stands for the cell membrane potential and x_2 and x_3 describe the ionic currents flowing across the membrane through fast and slow ion channels, respectively. The parameter $0 < \varepsilon \ll 1$ is small, which makes x_3 a slow variable. I represents the membrane input current and x_{rest} is the rest potential of the system. Having studied a limit cycle and a chaotic behaviour, we then choose in the HR model a complex transient trajectory where the two time scales interplay. The study of transient dynamics is

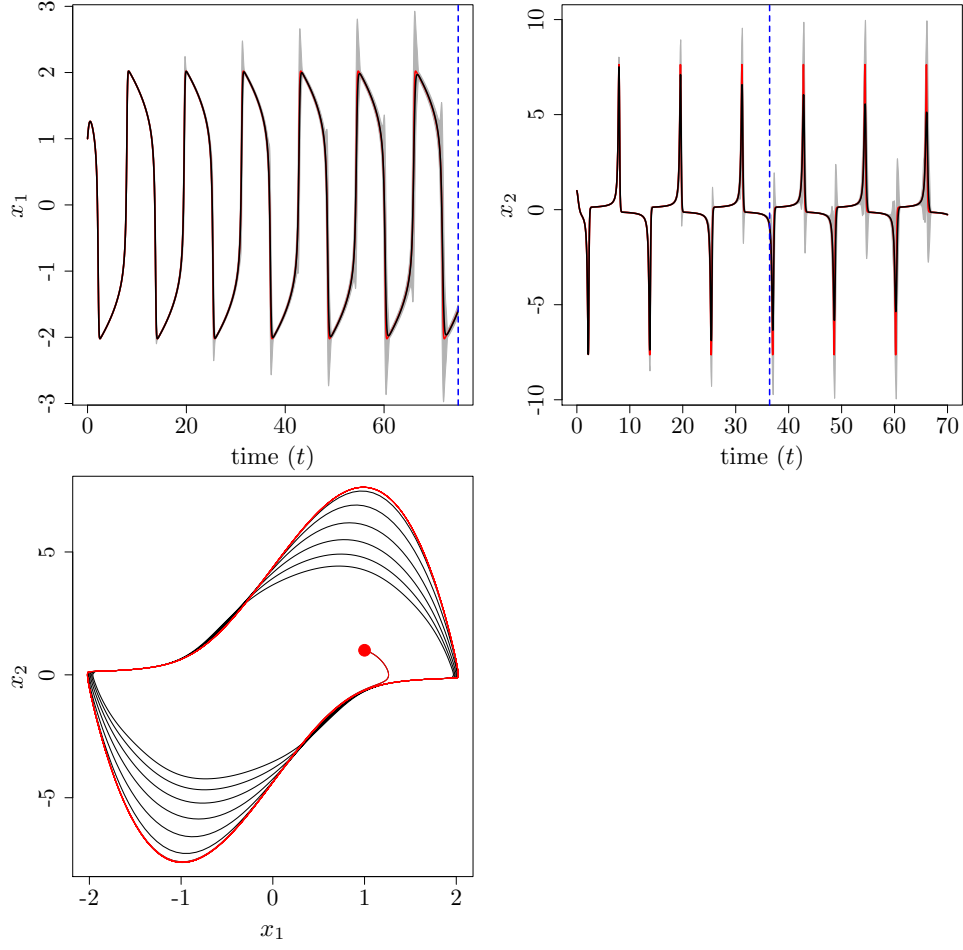


Figure 5: The van der Pol oscillator (red), the prediction (black) and credible interval (shaded) using Method 1. The dashed blue lines show the predictability horizon. The initial condition (red point) and parameter value are $\mathbf{x}_0 = (1, 1)^\top$ and $a = 5$.

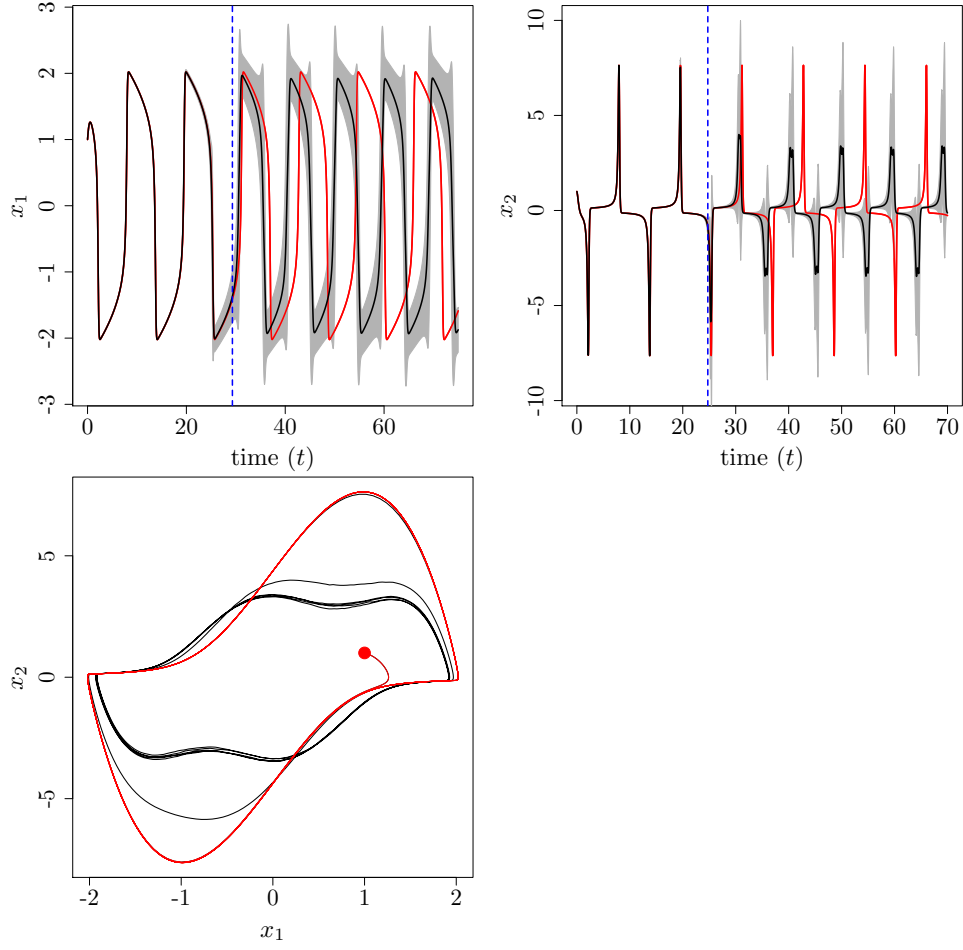


Figure 6: The van der Pol oscillator (red) and its emulation (black) using Method 2 where $\mathbf{x}_0 = (1, 1)^\top$ and $a = 5$. The dashed blue lines are the predictability horizons. A frequency miss-match happens after the predictability horizon and the amplitude of the predictions gradually damp.

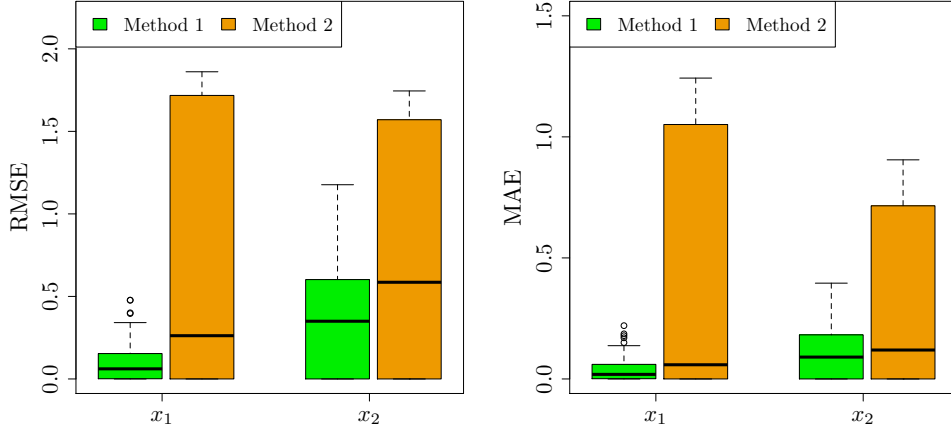


Figure 7: The box plot of MAE and RMS associated with Method 1 (green) and Method 2 (orange) in emulating the van der Pol equation. The two criteria are computed using 100 initial conditions selected randomly from $[-10, 10]^2$. The RMSE and MAE of Method 1 are significantly smaller than those of Method 2.

important in many real-world phenomena, see e.g. [20, 31]. To this end, in our experiments the value of the parameters ε , I and x_{rest} are set to 0.01, 2.4 and -1.6, respectively. The typical values for the constant parameters a_1, \dots, a_5 are: $a_1 = 1, a_2 = 2.7, a_3 = 1, a_4 = 5$ and $a_5 = 4$ [3]. These parameter values are considered in the examples below.

Figures 8 and 9 present the HR model (red), its prediction (black) and the associated uncertainty (shaded) based on Methods 1 and 2, respectively. The initial condition is $\mathbf{x}_0 = (1, 1, 1)^\top$ in both cases. We see that Method 1 has once again a superior performance compared to Method 2 in emulating all three state variables. In Method 1 the emulator remains reliable until the end of simulation and the predictability horizon is equal to 100. For further investigation, we compare the two algorithms based on the MAE and RMSE criteria using 100 (random) initial conditions. The box plot of the criteria is demonstrated in Figure 10. The results suggest that Method 1 yields a more accurate emulation of the HR model.

6 Conclusions

We proposed a novel data-driven approach for emulating deterministic complex dynamical systems implemented as computer codes. The output of such models is a time series and presents the evolving state of a physical phenomenon over time. Our method is based on emulating the short-time numerical flow map of the system and using the emulated flow map in an

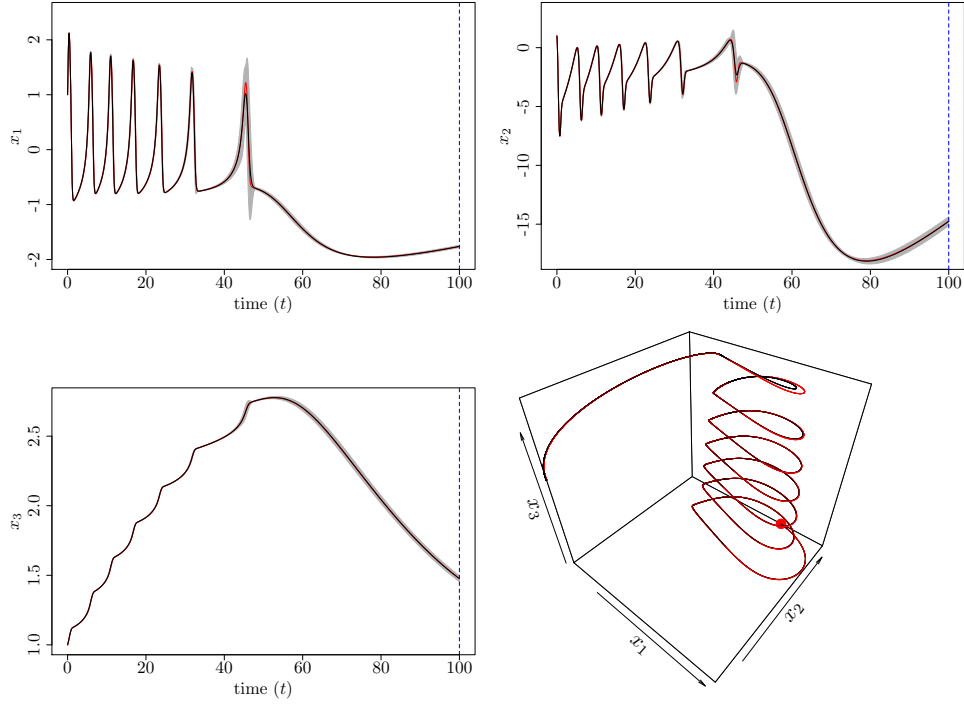


Figure 8: Emulating the HR model with the initial condition $\mathbf{x}_0 = (1, 1, 1)^\top$ based on Method 1. The proposed approach has a high prediction performance such that the difference between the truth (red) and emulation (black) is negligible. The predictability horizon (dashed blue) occurs at the end of the simulation for all three variables.

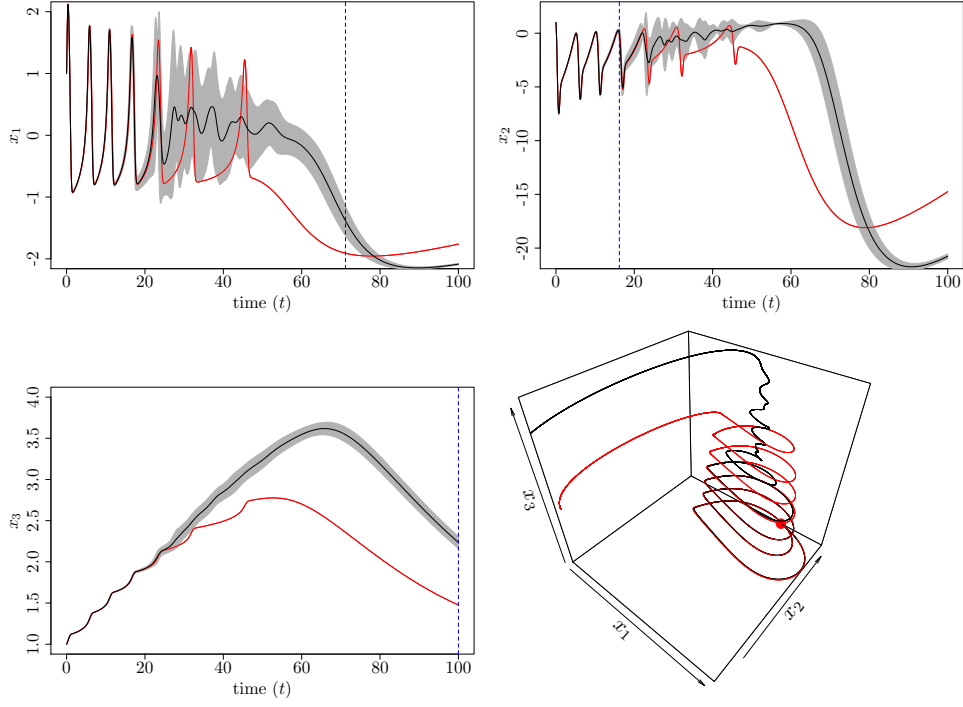


Figure 9: Emulating the HR model with the initial condition $\mathbf{x}_0 = (1, 1, 1)^\top$ using Method 2. The simulation and emulation are shown in red and black, respectively. This approach has a lower prediction performance compared to Method 1, see Figure 8.

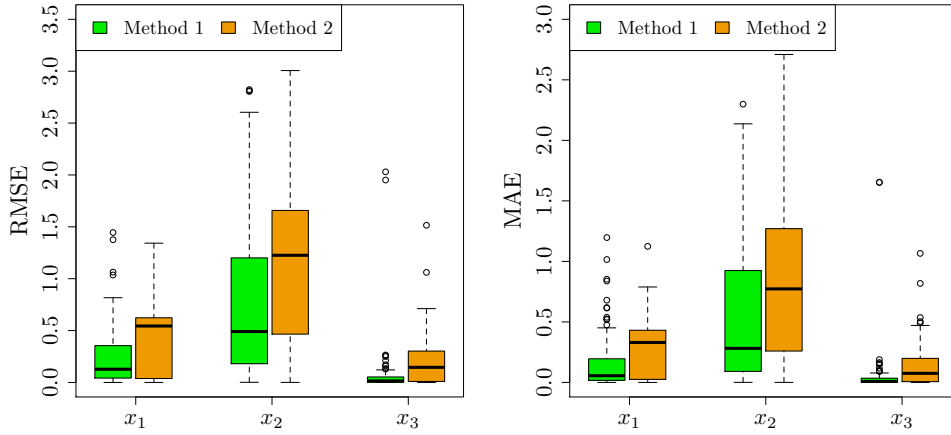


Figure 10: The box plot of MAE and RMS associated with Method 1 (green) and Method 2 (orange) using 100 different initial conditions chosen from $[-10, 10]^3$. Method 1 outperforms Method 2 in emulating the HR model.

iterative manner to perform one-step ahead predictions. The flow map is a function that returns the solution of a dynamical model at a certain time point, given initial conditions. In this paper, the numerical flow map is emulated via a GP whose kernel is approximated with random Fourier features. This yields a random predictor and allows us to draw multiple realisations from the approximate flow map. When the realisations are employed in the one-step ahead prediction paradigm, a distribution over the time series is created. The mean and variance of that distribution serve as the time series prediction and the associated uncertainty, respectively. The proposed method is tested on several non-linear dynamic simulators such as the Lorenz, van der Pol, and Hindmarsh-Rose models. The results suggest that our approach can emulate those systems accurately and the prediction uncertainty can capture the true trajectory with a good accuracy. A future work direction is to conduct quantitative studies such as uncertainty quantification and sensitivity analysis on computationally expensive dynamical simulators emulated by the method suggested in this paper.

Acknowledgments

HM and PC would like to thank the Alan Turing Institute for funding this work.

Appendix A Reproducing kernel Hilbert space

Let \mathcal{H} be a Hilbert space of functions defined on \mathcal{X} . The function $k(\cdot, \cdot)$ is called a reproducing kernel of \mathcal{H} , and \mathcal{H} is an RKHS, if it satisfies

1. $\forall \mathbf{x} \in \mathcal{X} \rightarrow k(\mathbf{x}, \cdot) \in \mathcal{H}$; and
2. $\forall \mathbf{x} \in \mathcal{X}$ and $\forall f \in \mathcal{H}$, $\langle f, k(\cdot, \mathbf{x}) \rangle_{\mathcal{H}} = f(\mathbf{x})$ (the reproducing property) .

For the reproducing kernel k and the feature map $\phi : \mathbf{x} \mapsto k(\mathbf{x}, \cdot)$, we have

$$\langle \phi(\mathbf{x}), \phi(\mathbf{x}') \rangle_{\mathcal{H}} = \langle k(\mathbf{x}, \cdot), k(\mathbf{x}', \cdot) \rangle_{\mathcal{H}} = k(\mathbf{x}, \mathbf{x}'), \quad \forall \mathbf{x}, \mathbf{x}' \in \mathcal{X}, \quad (22)$$

which follows directly from the reproducing property. The above equation suggests that the input space \mathcal{X} can be projected into a higher (or infinite) dimensional feature space (through ϕ) where the learning procedure can be more successful.

Appendix B Parameter estimation

The stochastic process $Y(\mathbf{x})$ depends on a set of parameters $\boldsymbol{\theta}$ that are generally unknown and need to be estimated from the data. Suppose that

$\boldsymbol{\theta} = \{\sigma^2, \boldsymbol{\beta}, \boldsymbol{\delta}\}$ is the set of parameters where $\boldsymbol{\delta} = [\delta_1, \dots, \delta_d]^\top$. We use the maximum likelihood method to estimate them. The logarithm of the likelihood function is

$$\mathcal{L}(\boldsymbol{\theta} \mid \mathbf{y}) = -\frac{n}{2} \ln(2\pi\sigma^2) - \frac{1}{2} \ln(|\mathbf{K}|) - \frac{1}{2\sigma^2} (\mathbf{y} - \boldsymbol{\mu})^\top \mathbf{K}^{-1} (\mathbf{y} - \boldsymbol{\mu}), \quad (23)$$

where the correlation matrix \mathbf{K} depends on $\boldsymbol{\delta}$ and $\boldsymbol{\mu} = \mathbf{Q}\boldsymbol{\beta}$ in which $\mathbf{Q} = [\mathbf{q}(\mathbf{x}^1), \dots, \mathbf{q}(\mathbf{x}^n)]^\top$. It is an $n \times r$ matrix called the *experimental matrix* and comprises the evaluation of the regression functions at the training data. An estimate of $\boldsymbol{\beta}$ and σ^2 is obtained by taking the derivatives of $\mathcal{L}(\boldsymbol{\theta} \mid \mathbf{y})$ with respect to those parameters and setting the derivatives to zero. The estimated parameters have closed-form expressions given by

$$\hat{\boldsymbol{\beta}} = (\mathbf{Q}^\top \mathbf{K}^{-1} \mathbf{Q})^{-1} \mathbf{Q}^\top \mathbf{K}^{-1} \mathbf{y}, \quad (24)$$

$$\hat{\sigma}^2 = \frac{1}{n} (\mathbf{y} - \mathbf{Q}\hat{\boldsymbol{\beta}})^\top \mathbf{K}^{-1} (\mathbf{y} - \mathbf{Q}\hat{\boldsymbol{\beta}}). \quad (25)$$

If the parameters $\boldsymbol{\beta}$ and σ^2 in Equation (23) are substituted with their estimates $\hat{\boldsymbol{\beta}}$ and $\hat{\sigma}^2$, the profile log-likelihood (after dropping the constants) is achieved as

$$\mathcal{L}_p(\boldsymbol{\delta} \mid \mathbf{y}) = -\frac{n}{2} \ln(\hat{\sigma}^2) - \frac{1}{2} \ln(|\mathbf{K}|). \quad (26)$$

Finally, the length-scales can be estimated by solving the optimisation problem below

$$\hat{\boldsymbol{\delta}} = \arg \max_{\boldsymbol{\delta}} \mathcal{L}_p(\boldsymbol{\delta} \mid \mathbf{y}). \quad (27)$$

References

- [1] Reza Alizadeh, Janet K. Allen, and Farrokh Mistree. Managing computational complexity using surrogate models: A critical review. *Research in Engineering Design*, 31(3):275–298, 2020.
- [2] Mauricio A. Álvarez and Neil D. Lawrence. Computationally efficient convolved multiple output Gaussian processes. *Journal of Machine Learning Research*, 12(41):1459–1500, 2011.
- [3] Roberto Barrio and Andrey Shilnikov. Parameter-sweeping techniques for temporal dynamics of neuronal systems: Case study of hindmarsh-rose model. *Journal of mathematical neuroscience*, 1:1–6, 2011.
- [4] M. J. Bayarri, J. O. Berger, J. Cafeo, G. Garcia-Donato, F. Liu, J. Palomo, R. J. Parthasarathy, R. Paulo, J. Sacks, and D. Walsh. Computer model validation with functional output. *The Annals of Statistics*, 35(5):1874–1906, 2007.

- [5] Sourabh Bhattacharya. A simulation approach to Bayesian emulation of complex dynamic computer models. *Bayesian Analysis*, 2(4):783–815, 2007.
- [6] Salomon Bochner. *Lectures on Fourier integrals*. Princeton University Press, 1959.
- [7] S.L. Brunton and J.N. Kutz. *Data-driven science and engineering: Machine learning, dynamical Systems, and control*. Cambridge University Press, 2019.
- [8] Erika Camacho, Richard Rand, and Howard Howland. Dynamics of two van der Pol oscillators coupled via a bath. *International Journal of Solids and Structures*, 41(8):2133–2143, 2004.
- [9] Rob Carnell. *lhs: Latin Hypercube Samples*, 2020. R package version 1.1.1.
- [10] A. Castelletti, S. Galelli, M. Ratto, R. Soncini-Sessa, and P.C. Young. A general framework for dynamic emulation modelling in environmental problems. *Environmental Modelling & Software*, 34:5 – 18, 2012.
- [11] Ricky T. Q. Chen, Yulia Rubanova, Jesse Bettencourt, and David K Duvenaud. Neural ordinary differential equations. In *Advances in Neural Information Processing Systems 31*, volume 31, pages 6571–6583. Curran Associates, Inc., 2018.
- [12] Victoria C. P. Chen, Kwok-Leung Tsui, Russell R. Barton, and Martin Meckesheimer. A review on design, modeling and applications of computer experiments. *IIE Transactions*, 38(4):273–291, 2006.
- [13] S. Conti, J. P. Gosling, J. E. Oakley, and A. O’Hagan. Gaussian process emulation of dynamic computer codes. *Biometrika*, 96:663–676, 2009.
- [14] Steo Conti and Anthony O’Hagan. Bayesian emulation of complex multi-output and dynamic computer models. *Journal of Statistical Planning and Inference*, 140(3):640–651, 2010.
- [15] P. Cvitanović, R. Artuso, R. Mainieri, G. Tanner, and G. Vattay. *Chaos: Classical and Quantum*. Niels Bohr Institute, Copenhagen, 2016.
- [16] F. DERNONCOURT, K. VEERAMACHANENI, and U. M. O’REILLY. Gaussian process-based feature selection for wavelet parameters: Predicting acute hypotensive episodes from physiological signals. In *2015 IEEE 28th International Symposium on Computer-Based Medical Systems*, pages 145–150, 2015.

- [17] Angela M. dos Santos, Sergio R. Lopes, and R.L.Ricardo L. Viana. Rhythm synchronization and chaotic modulation of coupled van der Pol oscillators in a model for the heartbeat. *Physica A: Statistical Mechanics and its Applications*, 338(3):335–355, 2004.
- [18] Kai-Tai Fang, Dennis K. J. Lin, Peter Winker, and Yong Zhang. Uniform design: Theory and application. *Technometrics*, 42(3):237–248, 2000.
- [19] Thomas E. Fricker, Jeremy E. Oakley, and Nathan M. Urban. Multivariate Gaussian process emulators with nonseparable covariance structures. *Technometrics*, 55(1):47–56, 2013.
- [20] Marc Goodfellow, Kaspar Schindler, and Gerold Baier. Self-organised transients in a neural mass model of epileptogenic tissue dynamics. *NeuroImage*, 59(3):2644–2660, 2012.
- [21] José Miguel Henrández-Lobato, Matthew W. Hoffman, and Zoubin Ghahramani. Predictive entropy search for efficient global optimization of black-box functions. In *Proceedings of the 27th International Conference on Neural Information Processing Systems*, NIPS’14, pages 918–926. MIT Press, 2014.
- [22] Dave Higdon, James Gattiker, Brian Williams, and Maria Rightley. Computer model calibration using high-dimensional output. *Journal of the American Statistical Association*, 103(482):570–583, 2008.
- [23] J. L. Hindmarsh and R. M. Rose. A model of neuronal bursting using three coupled first order differential equations. *Proceedings of the Royal Society of London*, 221(1222):87–102, 1984.
- [24] Thomas Hofmann, Bernhard Schölkopf, and Alexander J. Smola. Kernel methods in machine learning. *Annals of Statistics*, 36(3):1171–1220, 2008.
- [25] Gaofeng Jia and Alexandros A. Taflanidis. Kriging metamodeling for approximation of high-dimensional wave and surge responses in real-time storm/hurricane risk assessment. *Computer Methods in Applied Mechanics and Engineering*, 261-262:24–38, 2013.
- [26] Ruichen Jin, Wei Chen, and Timothy W. Simpson. Comparative studies of metamodeling techniques under multiple modeling criteria. *Structural and Multidisciplinary Optimization*, 23(1):1–13, 2001.
- [27] M.E. Johnson, L.M. Moore, and D. Ylvisaker. Minimax and maximin distance designs. *Journal of Statistical Planning and Inference*, 26(2):131–148, 1990.

- [28] Marc C. Kennedy and Anthony O’Hagan. Bayesian calibration of computer models. *Journal of the Royal Statistical Society: Series B (Statistical Methodology)*, 63(3):425–464, 2001.
- [29] R. Killick, P. Fearnhead, and I. A. Eckley. Optimal detection of change-points with a linear computational cost. *Journal of the American Statistical Association*, 107(500):1590–1598, 2012.
- [30] Rebecca Killick and Idris Eckley. changepoint: An R package for changepoint analysis. *Journal of Statistical Software*, 58(3):1–19, 2014.
- [31] Tim Kittel, Jobst Heitzig, Kevin Webster, and Jürgen Kurths. Timing of transients: quantifying reaching times and transient behavior in complex systems. *New Journal of Physics*, 19(8):083005, 2017.
- [32] Georg Lindergen. *Lectures on stationary stochastic processes*. Lund University Press, 2006.
- [33] Haitao Liu, Yew-Soon Ong, Xiaobo Shen, and Jianfei Cai. When Gaussian process meets big data: A review of scalable GPs. *IEEE Transactions on Neural Networks and Learning Systems*, 31(11):4405–4423, 2020.
- [34] Edward N. Lorenz. Deterministic nonperiodic flow. *Journal of Atmospheric Sciences*, 20:130–148, 1963.
- [35] David Machac, Peter Reichert, and Carlo Albert. Emulation of dynamic simulators with application to hydrology. *Journal of Computational Physics*, 313:352–366, 2016.
- [36] Siamak Mehrkanoon and Johan A.K. Suykens. Deep hybrid neural-kernel networks using random Fourier features. *Neurocomputing*, 298:46–54, 2018.
- [37] Hossein Mohammadi, Peter Challenor, and Marc Goodfellow. Emulating dynamic non-linear simulators using Gaussian processes. *Computational Statistics & Data Analysis*, 139:178–196, 2019.
- [38] Joaquin Quiñero Candela. *Learning with uncertainty - Gaussian processes and relevance vector machines*. PhD thesis, Technical University of Denmark, 2004.
- [39] Edgar E. Peters. A chaotic attractor for the s&p 500. *Financial Analysts Journal*, 47(2):55–62, 1991.
- [40] Ali Rahimi and Benjamin Recht. Random features for large-scale kernel machines. In *Advances in Neural Information Processing Systems*, pages 1177–1184. Curran Associates Inc., 2008.

- [41] M. Raissi, P. Perdikaris, and G.E. Karniadakis. Physics-informed neural networks: A deep learning framework for solving forward and inverse problems involving nonlinear partial differential equations. *Journal of Computational Physics*, 378:686–707, 2019.
- [42] Carl Edward Rasmussen and Christopher K. I. Williams. *Gaussian processes for machine learning (adaptive computation and machine learning)*. The MIT Press, 2005.
- [43] Andreas Raue, Marcel Schilling, Julie Bachmann, Andrew Matteson, Max Schelker, Daniel Kaschek, Sabine Hug, Clemens Kreutz, Brian D. Harms, Fabian J. Theis, Ursula Klingmüller, and Jens Timmer. Lessons learned from quantitative dynamical modeling in systems biology. *PLOS ONE*, 8(12):1–17, 2013.
- [44] M. J. Roberts, P. L. Vidale, C. Senior, H. T. Hewitt, C. Bates, S. Berthou, P. Chang, H. M. Christensen, S. Danilov, M.-E. Demory, S. M. Griffies, R. Haarsma, T. Jung, G. Martin, S. Minobe, T. Ringler, M. Satoh, R. Schiemann, E. Scoccimarro, G. Stephens, and M. F. Wehner. The benefits of global high resolution for climate simulation: Process understanding and the enabling of stakeholder decisions at the regional scale. *Bulletin of the American Meteorological Society*, 99(11):2341–2359, 2018.
- [45] Jerome Sacks, William J. Welch, Toby J. Mitchell, and Henry P. Wynn. Design and analysis of computer experiments. *Statistical Science*, 4(4):409–423, 1989.
- [46] T. J. Santner, Williams B., and Notz W. *The design and analysis of computer experiments*. Springer-Verlag, 2003.
- [47] Bernhard Scholkopf and Alexander J. Smola. *Learning with kernels: Support vector machines, regularization, optimization, and beyond*. MIT Press, Cambridge, MA, USA, 2001.
- [48] Bobak Shahriari, Kevin Swersky, Ziyu Wang, Ryan P. Adams, and Nando de Freitas. Taking the human out of the loop: A review of Bayesian optimization. *Proceedings of the IEEE*, 104(1):148–175, 2016.
- [49] Karline Soetaert, Thomas Petzoldt, and R. Woodrow Setzer. Solving differential equations in R: Package deSolve. *Journal of Statistical Software*, 33(9):1–25, 2010.
- [50] S.H. Strogatz. *Nonlinear dynamics and chaos*. Studies in nonlinearity. Sarat Book House, 2007.
- [51] Mark van der Wilk. *Sparse Gaussian process approximations and applications*. PhD thesis, University of Cambridge, 2019.

- [52] Marcelo Viana. What’s new on lorenz strange attractors? *The Mathematical Intelligencer*, 22:6–19, 2000.
- [53] Shangying Wang, Kai Fan, Nan Luo, Yangxiaolu Cao, Feilun Wu, Carolyn Zhang, Katherine Heller, and Lingchong You. Massive computational acceleration by using neural networks to emulate mechanism-based biological models. *Nature Communications*, 10(1):1–9, 2019.
- [54] Ziyu Wang. *Practical and theoretical advances in Bayesian optimization*. PhD thesis, University of Oxford, 2016.
- [55] James T. Wilson, Viacheslav Borovitskiy, Alexander Terenin, Peter Mostowsky, and Marc Peter Deisenroth. Efficiently sampling functions from Gaussian process posteriors. *ArXiv e-prints*, 2020.
- [56] Arthur T. Winfree. Biological rhythms and the behavior of populations of coupled oscillators. *Journal of Theoretical Biology*, 16(1):15–42, 1967.